Interpretation of optical emission in a strongly inhomogeneous PIAD environment

J Harhausen[1*], R-P Brinkmann[2], R Foest[1], S Gorchakov[1], A Ohl[1] and B Schröder[2]

[1] *Leibniz-Institut für Plasmaforschung und Technologie e.V., Felix-Hausdorff-Strasse 2, D-17489 Greifswald, Germany*

[2] *Lehrstuhl für Theoretische Elektrotechnik, Ruhr-Universität Bochum, Universitätsstrasse 150, D-44801 Bochum, Germany*

[*] *E-mail: harhausen@inp-greifswald.de*

Preliminary remark

This extended abstract is intended to present work in progress. As this text is not subject to a rigorous review process, it is not claimed to be free of errors or to point out the final solution to the questions addressed. However, the results discussed are part of a publication in preparation. Readers are kindly invited to attend the presentation 'OR2202' on Thu, 12/09/13, or to contact the first author for questions or comments.

1 Introduction

A variety of methods exists for the production of high quality optical coatings. These are for instance magnetron or ion beam sputtering, or thermal evaporation assisted by ion or plasma ion beam sources. The choice of a particular technique is due to the specific demands for tailoring the thin film properties such as homogeneity, refractive index, absorption, mechanical stress, porosity (optical shift), etc.. To allow for economic production of complex multilayer designs, the issue of reproducibility at the highest deposition rate possible has to be faced.

The plasma ion assisted deposition (PIAD) has been invented to avoid contamination of the process environment present when gridded ion sources are employed. One example for this approach is the Advanced Plasma Source (APS)[1] which holds a considerable market share in the field of optical coatings. The APS is a hot cathode (LaB_6) DC glow discharge with an auxiliary magnetic field, typically operated with argon. A high density ($n_e \sim 10^{12}\,\mathrm{cm}^{-3}$) and high temperature ($T_e \sim 20\,\mathrm{eV}$) plasma is generated in the source region ($V \sim 0.7\,\mathrm{l}$) and expands to the chamber ($V \sim 10^3\,\mathrm{l}$) which is held at high vacuum ($p \sim 2 \cdot 10^{-2}\,\mathrm{Pa}$). The expansion induces a strong drop of the plasma potential V_p which results in an acceleration of the ions towards the substrates. The setup is outlined in figure 1. By varying the discharge voltage (V_D=50..150 V), the magnetic field (B_{max}=10..40 mT) and the gas flux (Γ_{Ar}=2..20 sccm) different characterstics of the plasma ion beam are obtained, where typical ion energies are E_i=50..150 eV. Detailed information on the APS plasma can be found in [2, 3].

As is described in the references, various probe techniques were adopted to elucidate the mechanisms of plasma beam formation in this particular PIAD setup. In an earlier work [4] the approach of optical emission spectroscopy (OES) has been pursued. This paper contains a description of the diagnostic installation allowing for tomogrgaphic reconstruction of the local optical emission near the source exit. With a simple corona model n_e and T_e could be estimated for an Ar/He mixture. The interpretation of emission close to the APS is hampered by the lack of detailed knowledge of neutral density and temperature in this region.

In this extended abstract the preparation of a more elaborate approach using collisional radiative modelling is sketched. The new aspect is the consideration of a global electron energy probability function (EEPF) based on the nonlocal approximation [5]. This concept is useful for reducing the complexity of electron kinetics by coordinate transformation from the 6D phase-space to a 1D total energy space. The analysis of OES data is not merely ment as a proof of principle. The final goal is to interpret the OES data in terms of electron parameters, as a foundation of a control scheme for the APS using non-invasive optical diagnostics. Although global parameters, such as voltages and currents can be maintained accurately, drifts in the plasma parameters which are not measured routinely in the industrial application, may lead to limitations in the reproducibility of the optical coatings. The main reason is suspected to be the alteration of the electrodes of the APS during the PIAD process.

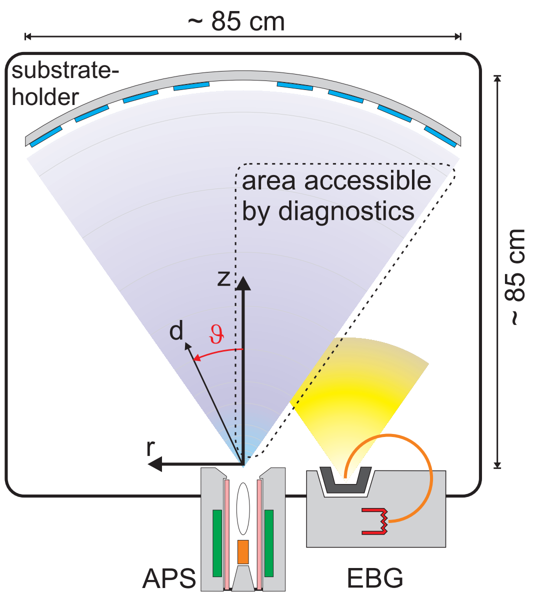

Figure 1: Scheme of the PIAD setup with plasma source (APS) and electron beam evaporator (EBG) at the bottom. The plasma diagnostics are positioned in the chamber by employing manipulators not shown in this figure. Note the indicated coordinate system.

2 Collisional radiative modelling

For argon, several approaches for collisional radiative (cr) modelling have been published, e.g. [6, 7]. Differences among the models are found in the number of species and energy levels considered, and the particular sets of cross section data adopted. Here, we use a cr-model being part of a code to resolve the electron kinetics in low pressure argon plasmas [8]. The model consideres 16 populations of argon species corresponding to the ground state $1s_1$, the first 14 excited states (in Paschen notation with increasing threshold energy: $1s_5$-$1s_2$, $2p_{10}$-$2p_1$) and the ion. In order to calculate the level/species populations, 121 cross sections for electron impact ionisation and excitation, 57 rate coefficients for quenching, 5 rate coefficients for chemoionization and 28 time constants for radiative decay are provided. Further, since the code is spatially 1D ('long discharge tube'), a radius of the plasma is defined, as well as transport parameters assigned to describe the diffusion of the ion and the metastable states ($1s_3$,$1s_5$) to the wall where the particles are neutralized or deexcited, respectively. The abundance of metastable states has a strong impact on the level populations which is one of the main problems for the development of a realistic cr-model. Here, it is aimed at finding trends based on the input data.

The code is employed to provide the argon excited states densities along the z-axis of the APS. As the neutral density, a fixed value of $n_0 = 2.5 \cdot 10^{12}\,\mathrm{cm}^{-3}$ is defined which is based on an estimate according to a background pressure of $p \sim 2 \cdot 10^{-2}\,\mathrm{Pa}$ in the chamber. For the model parameter tube-radius the diameter of the plasma at the particular z-position is considered. Although the whole process chamber is filled by the plasma, data from probes and the distribution of optical emission indicates that the plasma beam covers a cone-like region, as indicated in figure 1. At the low background pressure the mean free path of particles is quite large, so that species intersecting the plasma region from outside are assumed to be ground state neutrals originating from the vessel wall. The electron parameters are defined by the nonlocal EEPF and the ion density is set by the condition of quasi-neutrality.

3 Results and discussion

The results of the cr-model for one set of input data is presented. For brevity, we omit to state the APS configuration in detail which can be found in [3], section 4.1. Since the energy relaxation length for electrons is much larger than the dimension of the chamber, the nonlocal approximation holds. This is seen from the shape of the local EEPFs recorded along the z-axis. When these local EEPFs are plotted against the total energy of the electrons $E_{\mathrm{tot}} = E_{\mathrm{kin}} + E_{\mathrm{pot}}$, i.e. considering the magnitude of the local V_{p} one global EEPF containing all information can be deduced. Figure 2 shows such a nonlocal EEPF, together with the profile of $V_{\mathrm{p}}(z)$. The EEPF depicted represents the local EEPF at z=0 , if the abscissa is shifted by $+V_{\mathrm{p}}(z{=}0){=}65\,\mathrm{V}$. In general, the local EEPF is obtained by shifting the energy axis by $+V_{\mathrm{p}}(z_{\mathrm{i}})$ and considering the data according to the positive half space of the energy axis which corresponds to the kinetic energy of the electrons. The shape of the nonlocal EEPF indicates that the low energy electrons are distributed likewise maxwellian, while in the high energy region, the population is depleted. Most of the electrons are bound to the source region and only the high energy electrons a able to overcome the potential barrier towards larger distances from the source. The escaping electrons compensate the ion current to the chamber walls. Figure 3 gives an impression on the accuracy of the EEPF-model. The probe data for n_e and $T_{e,eff}(=2/3 \cdot \langle E_e \rangle)$ is well matched, albeit the high energy depletion is slightly underestimated, so that modelled and experimental values for n_e deviate at larger z-values.

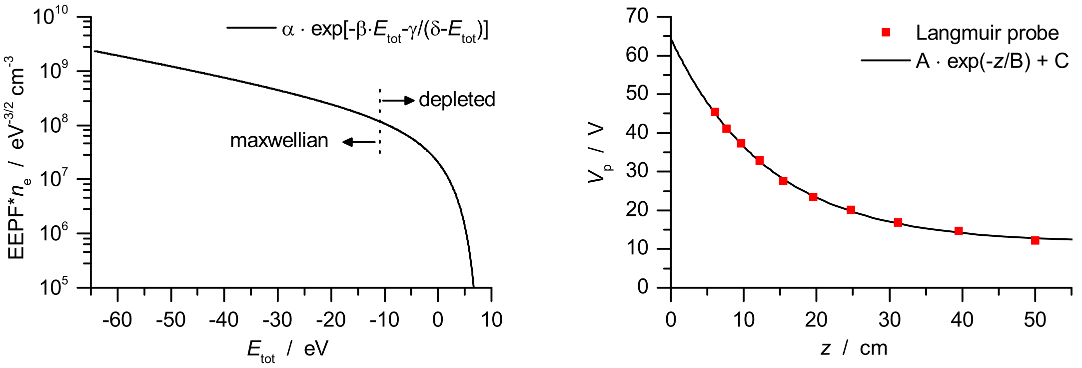

Figure 2: Models for the nonlocal EEPF (left) and for the profile of the plasma potential V_p (right) on the z-axis based on Langmuir probe data for a particular APS setting. $\{\alpha, \beta, \gamma, \delta\}$, $\{A, B, C\}$ are fitting parameters.

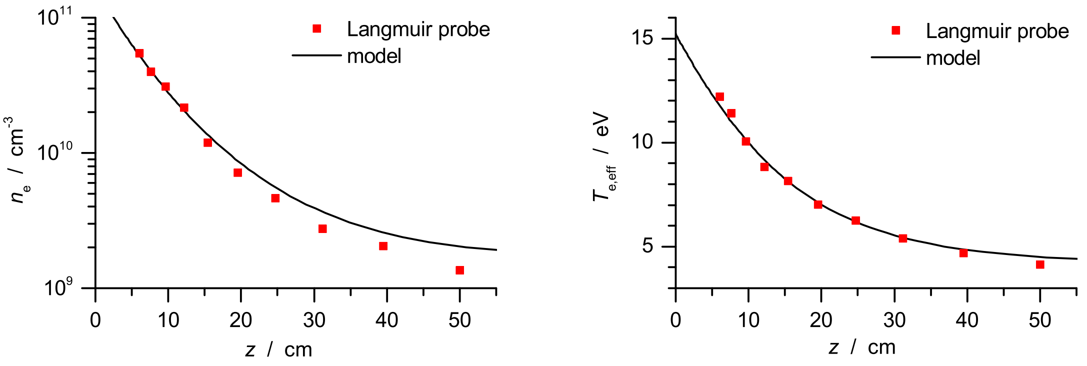

Figure 3: Electron density n_e (left) and effective electron temperature $T_{e,eff}$ (right) as determined by the Langmuir probe and the trends according to the models shown in figure 2.

The cr-code is used for a z-array which is accessible to the OES diagnostics. Figure 4 shows the resulting densities for the 1s and 2p states, where the latter are relevant for OES due to the VIS-NIR radiation. Unsurprisingly, there is a strong drop in density along the z-axis, because both n_e and $T_{e,eff}$ drop significantly. This is in agreement with the observation that the APS plasma is very bright near the source exit and the emission is barely detectable for $z > 20\,\mathrm{cm}$. The evolution of the 1s states, i.e. the slight difference between the profile shapes of metastable and non-metastable densities has a slight impact on the population of the 2p states. Since it can hardly be resolved in the $n_x(z)$-plot, ratios of densities are shown in the right part of figure 4. Most of the 2p density ratios do not exhibit a significant variation along z. This is clear from the point of view, that the 2p states have very similar threshold energies. In principle, line ratio techniques based on very different cross sections (shape and threshold) are employed to estimate T_e . However, the ratio $2p_9/2p_4$ varies by more than a factor of two. The actual emission connected to these 2p states should give an indication, whether the approach of the cr-model is reasonable. If the experimental data deviates strongly from the predictions of the model, it is likely the abundance of metastable states which is estimated incorrectly.

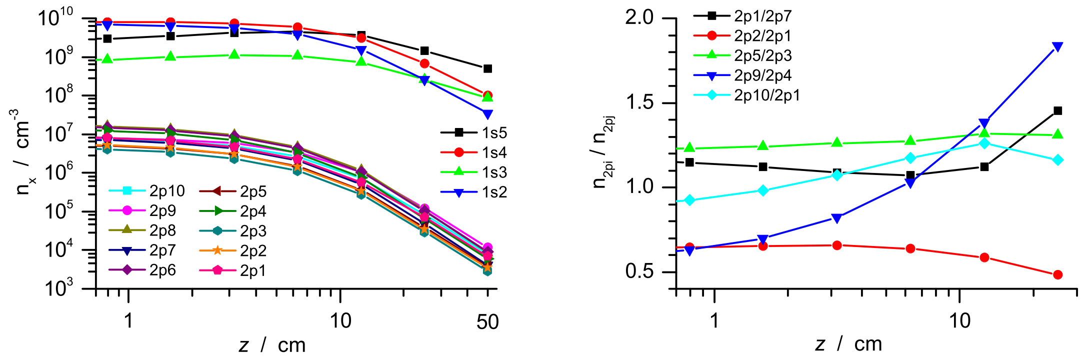

Figure 4: Left: Profiles of argon excited states densities obtained by the cr-model using the EEPF of figure 2 and further settings mentioned in the text. Right: Set of ratios of argon excited states densities.

4 Outlook

In an experimental campaign VIS/NIR line emission will be recorded and probe measurements conducted to optain the nonlocal EEPF. In order to use the cr-model reasonably, the neutral density near the APS exit will be estimated, based on the electron parameters known. The line emission predicted by the model will be compared to the experimental data. There are two approaches to check for consistency: (1) to consider the model being accurate and using as input the EEPF only to calculate the neutral density ; (2) to use the estimated neutral density, so the input to the code is EEPF and neutral density, thereby testing the reasonability of the cr-model itself.

The cr-model employed might be critizised as being too simple. Actually, emission from high lying excited neutral and ion states is observed experimentally, indicating significant densities of these states. The first goal is to examine whether global trends can be recovered from the cr-model. In order to exploit the experimental data more thoroughly, we also check whether a line ratio technique proposed for the estimation of T_e (3p states, see [9]) can be used successfully. A simple approach to monitor T_e close to the source would be a valuable tool for process optimization. Nevertheless, the ultimate goal is to determine the free parameters of the nonlocal EEPF-model by recording a proper set of argon lines during a PIAD process.

Acknowledgment

This work is funded by the German Federal Ministry of Education and Research (BMBF, Fkz. 13N10462).

References

[1] Matl K, Klug W, and Zöller A *Mat. Sci. Eng.* **A140** 523-7

[2] Schröder B, Brinkmann R P, Harhausen J, and Ohl A 2011 *J. Appl. Phys.* **110** 043305

[3] Harhausen J, Brinkmann R P, Foest R, Hannemann M, Ohl A, and Schröder B 2012 *Plasma Sources Sci. Technol.* **21** 035012

[4] Harhausen J, Meyenburg I, Ohl A, and Foest R 2011 *Surf. Coat. Tech.* **205** S407-10

[5] Kortshagen U, Busch C, and Tsendin L D 1996 *Plasma Sources Sci. Technol.* **5** 1-17

[6] Vlcek J 1989 *J. Phys. D: Appl. Phys.* **22** 623-31

[7] Bogaerts A, Gijbels R, and Vlcek J 1998 *J. Appl. Phys.* **84** 121-36

[8] Gorchakov S, Loffhagen D, and Uhrlandt D 2006 *Phys. Rev. E* **74** 066401

[9] Boffard J B, Jung R O, Lin C C, Aneskavich L E, and Wendt A E 2012 *J. Phys. D: Appl. Phys.* **45** 045201